Applied Physics B
Lasers and Optics

CrossMark

Modeling of the static and flowing-gas ring-LD side-pumped alkali vapor amplifiers

Binglin Shen[1] · Xingqi Xu[1] · Chunsheng Xia[1] · Bailiang Pan[1]

Abstract A new method of pump-coupling in diode-pumped alkali vapor amplifier is reported, which uses ring-LD to tightly surround the alkali vapor cell for directly coupled side-pumping. The kinetic and fluid dynamic modeling, numerical approaches of the ring-LD side-pumped configuration are proposed and applied to the static and the flowing-gas Cs vapor amplifiers. Pump intensity and temperature distribution in the cell are simulated. Influences of some important factors on laser power are calculated and analyzed. Comparisons of different pumped configurations are made, demonstrating the highest utilizing efficiency of pump power of the ring-LD side-pumped configuration. Thus the model is very helpful for designing high-power side-pumped alkali vapor amplifiers.

1 Introduction

High efficiency and high power in a high-quality beam, which is desirable for various important applications in science, technology and national security areas, are the important research targets of laser, and diode-pumped alkali vapor lasers (DPALs), having been extensively studied during the past dozen years, are thought to have the potential to achieve these goals. Up to now, via the use of high-power laser diode (LD) and flowing-gas configuration, the output power of DPALs has reached kW level, demonstrating its potential for power scaling [1–9].

Using master oscillator power amplifier (MOPA) is an effective approach to further improve the power of DPALs. Up to now, some MOPA experiments on DPALs have been made [10–13] and their corresponding models were setup [14–19], which agreed well with experimental results. However, in spite of these experiments and theoretical works, study on ring-LD side-pumped configuration which can accomplish directly coupled side-pumping in alkali vapor amplifier is still absent.

Illuminating the alkali vapor cell from all the sides by ring-LD surrounding the cell, which can help to improve the utilizing efficiency of pump energy, is suggested for the first time. Our model for ring-LD side-pumped alkali vapor amplifiers takes into account not only the temperature rise, the amplified spontaneous emission and the saturation effect, but also the processes of the alkali atoms excitation to high electronic levels, the ionization of these levels, and the electron–ion recombination. Fluid dynamic processes [20–22] are also included when it is applied to the flowing-gas case, thus the model is able to describe both low-power static and high-power flowing-gas configurations.

2 Modeling of a ring-LD side-pumped alkali vapor amplifier

The schematic diagram of a ring-LD side-pumped alkali vapor laser MOPA system is shown in Fig. 1. As most of the experiments, the amplifier cell is designed into a hollow cylinder ($R \times L$), covered by a quartz tube heater and contains a mixture of alkali vapor and buffer gases at operation temperature. The ring-LD installed on heat sinks is made up of two semi-ring laser diode arrays. The pump lights from the ring-LD enter the cell in the side, while the seed laser from the master oscillator enters into the cell from the

✉ Bailiang Pan
   pbl66@zju.edu.cn

[1] Department of Physics, Zhejiang University,
   Hangzhou 310027, China

Fig. 1 Schematic diagram of an alkali vapor amplifier in ring-LD side-pumped configuration
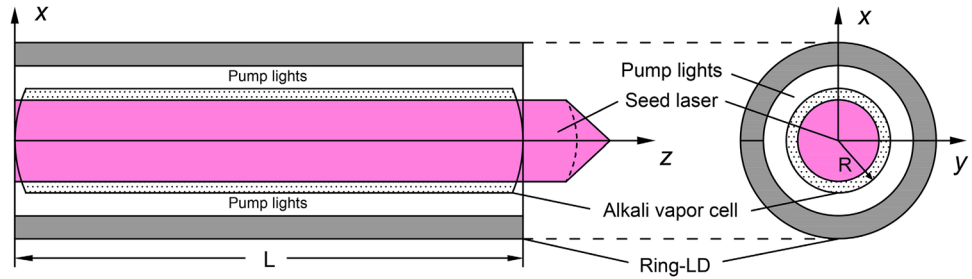
end and propagates along z-axis to be amplified. Both of them are assumed to be symmetric in respect to the optical axis.

2.1 Numerical approaches for pump power distribution

An iterative algorithm proposed to solve for the distributions of pump energy, temperature and population densities in the ring-LD side-pumped alkali vapor amplifier is described as follows:

The vapor cell is divided into many coaxial cylindrical annuli with a thickness of dr ($dr \ll R$) as shown in Fig. 2. The pump lights from ring-LD, P_p^+, move forward one bit step dr at a time, when they pass through the central core, if not being completely absorbed, they will keep on propagating and become P_p^- in the opposite direction. Thus in every divided cylindrical annulus, there are two pump powers P_p^+ and P_p^- with a homogeneous distribution on the outer surface and the inner surface, respectively.

In each divided cylindrical annulus, the rates of laser emission rate W_{21}, amplified spontaneous emission W_{ase}, relaxation W_{32}, spontaneous emission S_{31}, S_{21} and S_{km}, quenching Q_{m1}, photoexcitation I_{mk}, energy pooling Po_{mk}, photoionization Ph_k, penning ionization Pn and recombination R^+, R_2^+ are all taken into account and being included in the rate equations given by [18].

The propagation equations of the forward and backward pump powers from the jth cylindrical annulus to the $(j + 1)$th one are given by

$$
P_p^+(i, j + 1, \lambda) = P_p^+(i, j, \lambda) \exp\left\{-\left[n_1(i,j) - \frac{1}{2}n_3(i,j)\right]\sigma_{D2}(i,j,\lambda)dr\right\},
$$

(1)

$$
P_p^-(i, j + 1, \lambda) = P_p^-(i, j, \lambda) \exp\left\{\left[n_1(i,j) - \frac{1}{2}n_3(i,j)\right]\sigma_{D2}(i,j,\lambda)dr\right\},
$$

(2)

where $\sigma_{D2}(i, j, \lambda)$ is the spectrally resolved atomic absorption cross section. i is the cycle index of the iterative process.
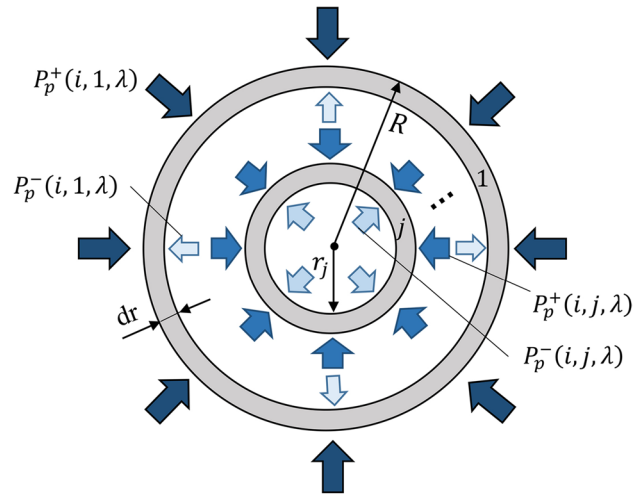
Fig. 2 Cross-sectional geometry of the ring-LD side-pumped amplifier cell

In the jth cylindrical annulus, the expressions of pump absorption rate $W_{13}(i, j)$ can be expressed as

$$
\begin{aligned}
W_{13}(i,j) = &\frac{1}{h v_p V_p(j)} \int P_p^+(i, j, \lambda) \\
&\times \left\{1 - \exp\left[-(n_1(i,j) - \frac{1}{2}n_3(i,j))\sigma_{D2}(i,j,\lambda)dr\right]\right\}d\lambda \\
&+ \frac{1}{h v_p V_p(j)} \int P_p^-(i, j, \lambda) \\
&\times \left\{\exp\left[(n_1(i,j) - \frac{1}{2}n_3(i,j))\sigma_{D2}(i,j,\lambda)dr\right] - 1\right\}d\lambda
\end{aligned}
$$

(3)

where $h v_p$ and $h v_l$ are the pump and the laser photon energy, respectively. $V_p(j)$ and $V_l(j)$, which denote the volume of the pump laser and the amplified laser are assumed to be equal to the volume of the jth cylindrical annulus.

The power distribution of the seed laser is modeled as having a two-dimensional Gaussian spectral profile given by

$$
P_s(j) = P_{sl} \frac{2S(j)}{\pi \omega_s^2} \exp\left(\frac{-2r_j^2}{\omega_s^2}\right),
$$

(4)

where P_{sl} and ω_s are the total power and beam waist of the seed laser, while $S(j)$ is the cross-sectional area of the jth cylindrical annulus.

First, we let the pump lights from the ring-LD pass through the gain medium until reach the central core, which means

$$P_p^-(1, j, \lambda) = 0. \tag{5}$$

Then let the unabsorbed pump power in the center $P_p^+(i, N + 1, \lambda)$ (N is the ordinal number of the final cylindrical annulus) pass the gain medium through the population distribution just calculated, and we can obtain the unabsorbed pump power on the surface of the cell, which is exactly the power of backward propagating pump lights, thus $P_p^-(i, j, \lambda) = P_p^+(i, 2N + 2 - j, \lambda)$. The total pump power in a cylindrical annulus should be

$$P_p^{tot}(i, j, \lambda) = P_p^+(i, j, \lambda) + P_p^-(i, j, \lambda). \tag{6}$$

Now use the total pump power to calculate the new population distribution $n(i + 1, j)$ and compare it with the old one $n(i, j)$, and if they are basically equal (<0.1 %), then we get the final solution. If not, repeat the prior steps, and continue the iterative process until the population distribution keeps constant.

2.2 Numerical approaches for temperature distribution

For high-power flowing-gas diode-pumped alkali vapor amplifier, the fluid dynamic processes in the annuli should also be taken into account. According to [18, 22], the generated heat $G(i, j)$ due to relaxation between the fine-structure levels and their quenching is given by

$$G(i, j) = V_l(j)\left[W_{32}(i, j)\Delta E + h\nu_l Q_{21}(i, j) + h\nu_p Q_{31}(i, j)\right], \tag{7}$$

where $h\nu_l$ is the laser photon energy.

The flowed heat removal $F(i, j)$ in a cylindrical annulus can be calculated by

$$F(i, j) = \frac{uS(j)n_g(i, j)}{N_A}\int_{T_w}^{T(i,j)} C_p(T')\mathrm{d}T', \tag{8}$$

where u and $n_g(i, j)$ denote the velocity and number density of the total mixed gases in the cell, respectively. N_A presents the Avogadro constant. $C_p(T)$ is the average molar heat capacity of the total buffer gases given by [18, 22].

When the thickness $\mathrm{d}r$ of a divided cylindrical annulus is sufficiently small, the conducted heat from the jth cylindrical annulus to the $(j - 1)$th one can be approximately expressed as

$$\Phi(i, j) = -K(i, j) \cdot 2\pi r_{j-1} l \frac{T(i, j) - T(i, j - 1)}{r_j - r_{j-1}}, \tag{9}$$

where $K(i, j)$ is the thermal conductivity given by [18, 22]. $T(i, 0) = T_w$ and $r_0 = R$.

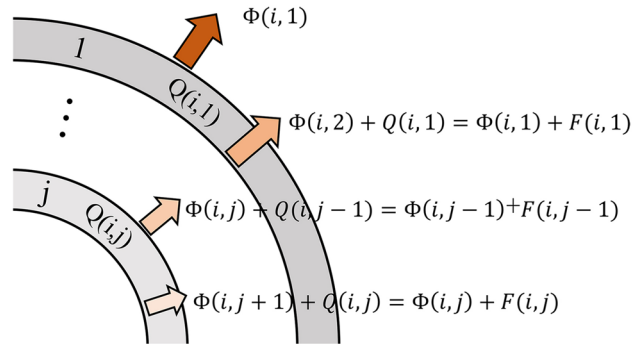As shown in Fig. 3, the energy balance that assuming the sum of the generated heat $G(i, j)$ and the conducted heat

Fig. 3 Schematic illustration of thermal balance in the cross section of the amplifier cell
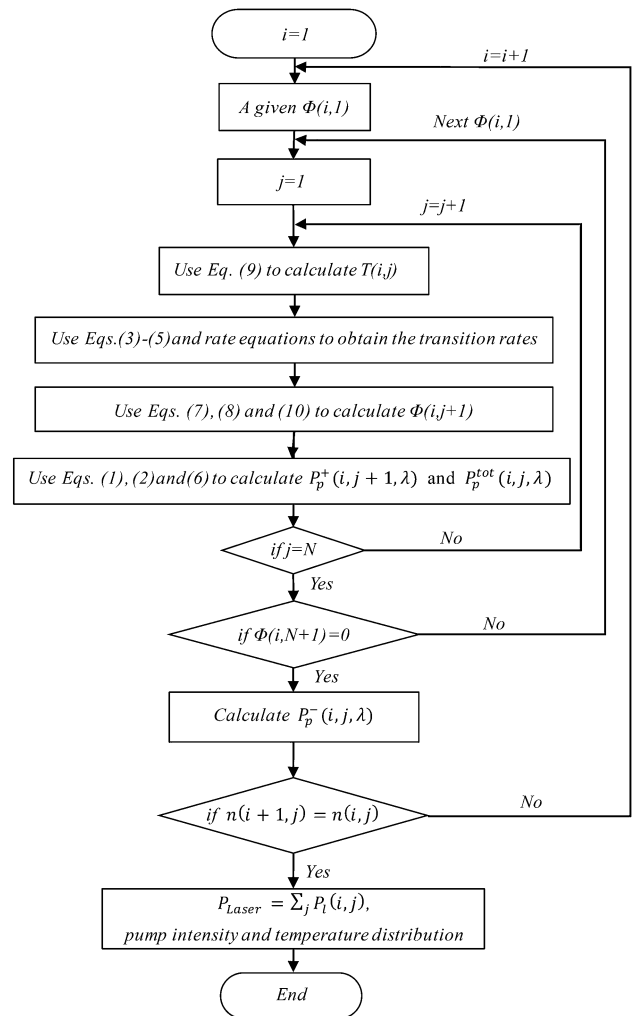

Fig. 4 Flowchart of the process of iterative algorithm for ring-LD side-pumped configuration

$\Phi(i, j + 1)$ from the $(j + 1)$th cylindrical annulus to the jth one is equal to the sum of the flowed heat $F(i, j)$ and conducted heat $\Phi(i, j)$ from the jth cylindrical annulus to the $(j - 1)$th one is given by

$$G(i,j) + \Phi(i, j+1) = F(i,j) + \Phi(i,j). \tag{10}$$

By giving an initial value of the conducted heat $\Phi(i, 1)$ and using the known wall temperature T_w, we can use the equation of conducted heat to solve the temperature of the first annulus $T(i, 1)$, then use it to solve the rate equations by which we can get the transition rates, and substitute them into generated heat $G(i, j)$ with flowed heat $F(i, j)$ to solve Eq. (10) by which we can obtain $\Phi(i, 2)$. Repeat this iterative process until we get the final conducted heat $\Phi(i, N + 1)$, if it is equal to zero, which means

$$\Phi(i, 1) = \sum_{j=1}^{N} Q(i,j) - \sum_{j=1}^{N} F(i,j), \tag{11}$$

then our appointed value of $\Phi(i, 1)$ is correct. Otherwise, repeat the prior steps by using the next value of $\Phi(i, 1)$ until the final solution is found.

A flowchart for explaining the process of the iterative algorithm described above is diagramed in Fig. 4.

3 Simulation results and discussion

3.1 Static, non-flowing-gas Cs vapor amplifier

There is rare experiment on side-pumped DPAL MOPA system, one is a single-side pumped Cs vapor amplifier with an entire cell held inside a custom cylindrical diffuse reflector to ensure homogeneous pumping [12], thus for comparison we use its experimental parameters described as follows: the cylindrical glass cell with dimensions of $R \times L = 0.35 \times 5$ cm is filled with 500 Torr ethane (measured at 20 °C). The seed laser power is 5 W with a 5 mm diameter. The pump power is 280 W with a linewidth (FWHM) of 10 GHz.

Dependence of the amplifier power on the oscillator power at an operating temperature of 103 °C is shown in Fig. 5. We can see that the simulation result of the ring-LD side-pumped amplifier agrees well with the experimental result of a single-side pumped amplifier with a cell surrounded by a diffuse type hollow cylinder reflector, this is because both of them have a quasi-homogeneous distribution of pump energy. The output power increases with increasing the seed power and slowly approaches saturation. The highest value of power achieved by these two configurations is almost equal.
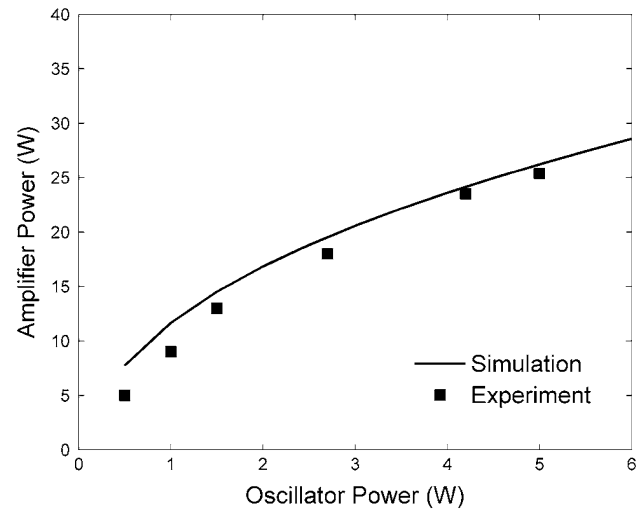
Fig. 5 Dependence of the output power on the input seed power when $T_w = 103$ °C
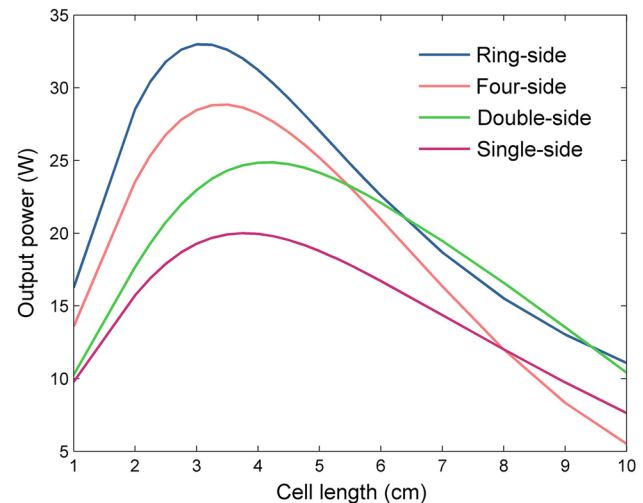
Fig. 6 Dependences of cell length on output power for different side-pumped configurations

However, Fig. 5 does not show the advantage of the ring-LD side-pumped configuration, thus an optimization of parameters is necessary to be discussed as follows.

Comparison of different side-pumped configurations is made and shown in Fig. 6 at an optimal temperature of 105 °C and a seed power of 5 W, and the length of the diode pumps is matched with the one of the cell. It can be seen from the figure that for every kind of side-pumped configurations there is an optimal length L_o where the output power is maximal. For example, for ring-LD side-pumped configuration, $L_o = 3$ cm, while for single-side pumped

configuration of which the cell has a slit (two symmetrical slits for double sides, four symmetrical slits for four sides [17]) parallel to the optical axis in the side for pump beams to enter through, 3.7 cm is needed.

When $L < 5.5$ cm, the values of the output power calculated for different configurations have the following relation: $P_{rs} > P_{4s} > P_{2s} > P_{1s}$, where the subscripts rs, 4s, 2s and 1s indicate ring-side, four-side, double-side and single-side pumped configuration, respectively. The calculated output power of ring-side pumped configuration, which can provide a more homogeneous distribution of pump power in the cell, is larger than those of the other three configurations.

3.2 Flowing-gas Cs vapor amplifier

To apply the model to a high-power flowing-gas Cs vapor amplifier, we consider a cylindrical vapor cell filled with the same pressures of ethane and helium as a flowing-gas Cs DPAL in [6]. The pump power $P_p = 1$ kW, the flowed velocity of the mixed gases $u = 10$ m/s, the wall temperature $T_w = 120$ °C, the cell radius $R = 3.5$ mm and the cell length $L = 5$ cm. The seed power is assumed to be 20 W with a beam waist of 2.5 mm.
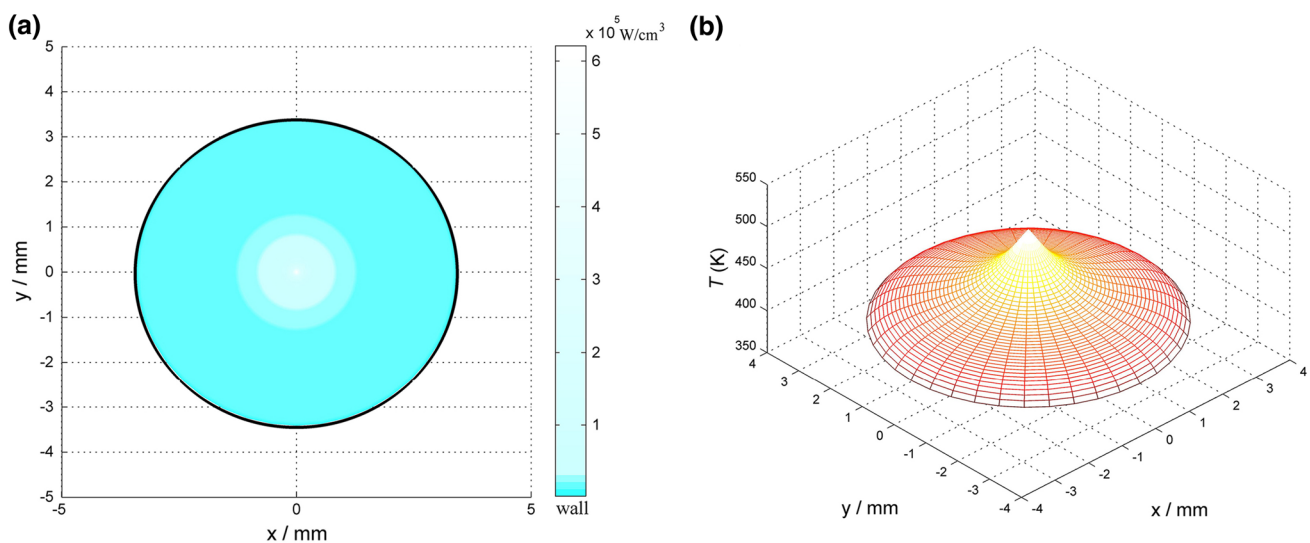
The pump energy and temperature distributions inside the vapor cell are theoretically calculated as shown in Fig. 7a, b, respectively. We can see that for ring-LD side-pumped configuration the pump intensity in the cell has a homogeneous distribution (10^4 W/cm^3) except the central area, that is obviously because the pump lights from all directions are converged here, making the pump intensity as well as the temperature in the central area much higher

than they are elsewhere in the cell, and reach maximum at the optical axis.

It can be seen from Fig. 7b that the temperature distribution has a distinct gradient in the cross section of the vapor cell with a high pump power, and the temperature peak appears at the center of the cross section, which is similar to the end-pumped DPAL in [22]. At the optical axis, the temperature is 500 K, while at the cell wall it falls to 393 K. Additionally, high flowing velocity can reduce the temperature difference and hence increasing the amplification factor, which is shown in the next figure.

Lowering the temperature gradient properly will be helpful for weakening the thermal effects [20]. Thus here, we simulated the dependences of the output power and radial temperature distribution on the longitudinal flow velocity u as shown in Fig. 8a, b, respectively. We can see that the output power dramatically grows with u and quickly saturates at $u \sim 10$ m/s, and between the smallest u and the largest u the difference of output powers can reach 16 % of pump power. Therefore, for $P_p = 1$ kW, a flow velocity of 10 m/s is need for efficient operation.

It can also be found from the figure that the absorbed pump energy has led to a more significant temperature rise if the mixed gases are not flown, this can be explained that the generated heat is totally transferred to the outside in a static cell by thermal conduction, which is far smaller in comparison with the convection. For this case the central temperature can even reach 869 K, much higher than the wall temperature, but still lower than the one of end-pumped DPAL in [22] because of homogeneous pumping. Flowing approach can effectively lower the temperature in the cell as shown in Fig. 8b, the temperature gradient

Fig. 7 Pump intensity (**a**) and temperature distribution (**b**) in the cell of a high-power flowing-gas ring-LD side-pumped amplifier

(a)

(b)
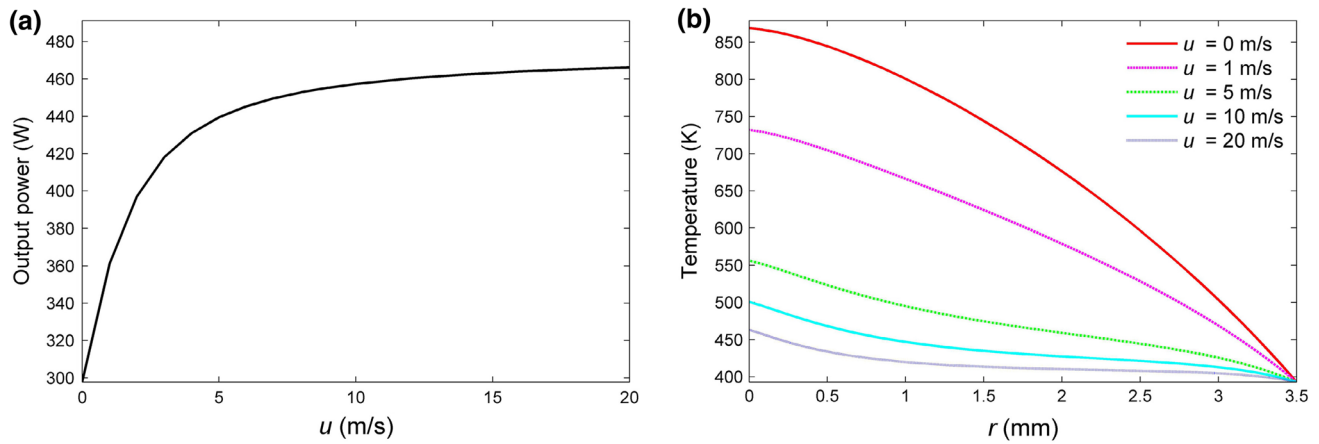
Fig. 8 Dependences of the output power (**a**) and radial temperature distribution (**b**) on u in the flowing-gas ring-LD sided-pumped alkali vapor amplifier
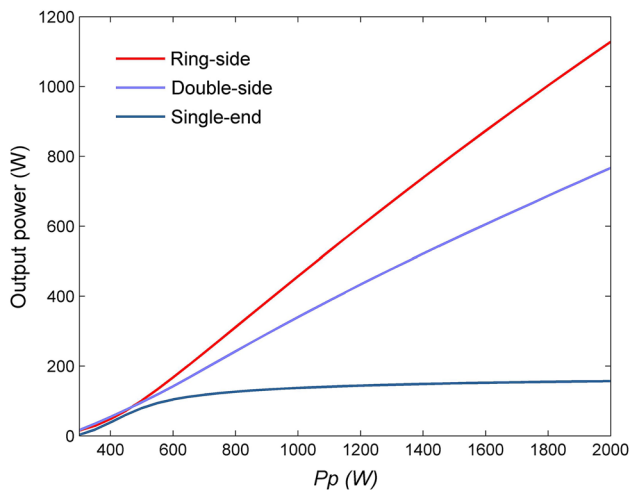
Fig. 9 Output power as function of pump power for alkali vapor amplifiers in single-end, double-side and ring-side pumped configuration with $u = 10$ m/s

decreases with the increasing u from ~ 476 K at $u = 0$ m/s to ~ 70 K at $u > 10$ m/s.

Comparison of the output performance of alkali vapor amplifiers in single-end, double-side and ring-side pumped configurations is presented in Fig. 9. For the former two configurations, the calculations were performed at an optimal wall temperature of 383 K and cell length of 8 cm [18], while for the ring-side pumped configuration, a higher temperature of 393 K but smaller cell length of 5 cm is chosen. At $P_p < 500$ W, the values of the output power calculated for different configurations are roughly equal, while at higher Pp, the output power of different configurations has the following relation: $P_{rs} > P_{2s} > P_{1e}$, where the subscripts rs and 2s indicate the same meaning above, while 1e indicate the single-end pumped configuration. The ring-LD

side-pumped configuration with a more homogeneous distribution of pump energy can achieve the highest output power, for example, at $P_p = 2$ kW, $P_{rs} = 1100$ W, while $P_{2s} = 760$ W and $P_{1e} = 150$ W, which demonstrates its advantage definitely.

4 Conclusion

A computational model with an iterative algorithm to describe the kinetic and fluid dynamic processes of a ring-LD side-pumped alkali vapor amplifier is reported, which takes into account the amplified spontaneous emission, the saturation effect, the excitation of the alkali atoms to high electronic levels, the ionization, and the heat generation and transfer in the gain medium. The simulation results were calculated and compared with the experiment results of a single-side pumped configuration with a custom cylindrical diffuse reflector to ensure quasi-homogeneous distribution of the pump energy.

Dependence of cell length on output power for different side-pumped configurations shows that at their own respective optimal cell length, amplifier with a more homogeneous distribution of the pump energy can achieve a higher value of output power. Especially, ring-LD side-pumped amplifier can achieve the best performance.

Simulation of pump intensity and temperature distribution in the cell shows that both of them turn out to be high in the center and low at the wall. A higher velocity of the flowing gas will result in a more homogeneous distribution of temperature and a substantial increase of amplified power. Dependences of output power on pump power in single-end, double-side and ring-side pumped configurations have again demonstrated the greatest capability of the ring-LD side-pumped amplifier to amplify the seed

power. Therefore, our model can provide an effective way to design an efficient side-pumped alkali vapor amplifier.

References

1. B.V. Zhdanov, R.J. Knize, Diode pumped alkali lasers. Proc. SPIE **8187**, 818707 (2011)
2. W.F. Krupke, R.J. Beach, V.K. Kanz, S.A. Payne, Resonance transition 795-nm rubidium laser. Opt. Lett. **28**(23), 2336–2338 (2003)
3. B.V. Zhdanov, A. Stooke, G. Boyadjian, A. Voci, R.J. Knize, Rubidium vapor laser pumped by two laser diode arrays. Opt. Lett. **33**(5), 414–415 (2008)
4. T. Ehrenreich, B. Zhdanov, T. Takekoshi, S.P. Phipps, R.J. Knize, Diode pumped caesium laser. Electron. Lett. **41**(7), 415–416 (2005)
5. B. Zhdanov, C. Maes, T. Ehrenreich, A. Havko, N. Koval, T. Meeker, B. Worker, B. Flusche, R.J. Knize, Optically pumped potassium laser. Opt. Commun. **270**(2), 353–355 (2007)
6. A.V. Bogachev, S.G. Garanin, A.M. Dudov, V.A. Eroshenko, S.M. Kulikov, G.T. Mikaelian, V.A. Panarin, V.O. Pautov, A.V. Rus, S.A. Sukharev, Diode-pumped caesium vapour laser with closed-cycle laser-active medium circulation. Quantum Electron. **42**(2), 95 (2012)
7. G.D. Hager, G.P. Perram, A three-level analytic model for alkali metal vapor lasers: part I. Narrowband optical pumping. Appl. Phys. B **101**(1–2), 45–56 (2010)
8. G.D. Hager, G.P. Perram, A three-level model for alkali metal vapor lasers. Part II: broadband optical pumping. Appl. Phys. B **112**(4), 507–520 (2013)
9. B. Shen, B. Pan, J. Yang, A. Qian, J. Jiao, Definition and analysis of the lineshape matching coefficient in diode-pumped alkali vapor lasers. Appl. Phys. B **117**(3), 817–822 (2014)
10. D.A. Hostutler, W.L. Klennert, Power enhancement of a rubidium vapor laser with a master oscillator power amplifier. Opt. Express **16**(11), 8050–8053 (2008)
11. B.V. Zhdanov, R.J. Knize, Efficient diode pumped cesium vapor amplifier. Opt. Commun. **281**(15), 4068–4070 (2008)
12. B.V. Zhdanov, M.K. Shaffer, R.J. Knize, Scaling of diode-pumped Cs laser: transverse pump, unstable cavity, MOPA. Proc. SPIE **7581**, 75810F (2011)
13. Y. Li, W. Hua, L. Li, H. Wang, Z. Yang, X. Xu, Experimental research of a chain of diode pumped rubidium amplifiers. Opt. Express **23**(20), 25906–25911 (2015)
14. B. Pan, Y. Wang, Q. Zhu, J. Yang, Modeling of an alkali vapor laser MOPA system. Opt. Commun. **284**(7), 1963–1966 (2011)
15. J. Yang, B. Pan, Y. Yang, J. Luo, A. Qian, Modeling of a diode side pumped cesium vapor laser MOPA system. IEEE J. Quantum Electron. **50**(3), 123–128 (2014)
16. Z. Yang, H. Wang, Q. Lu, W. Hua, X. Xu, Modeling of an optically side-pumped alkali vapor amplifier with consideration of amplified spontaneous emission. Opt. Express **19**(23), 23118–23131 (2011)
17. B. Shen, B. Pan, J. Jiao, C. Xia, Modeling of a diode four-side symmetrically pumped alkali vapor amplifier. Opt. Express **23**(5), 5941–5953 (2015)
18. B. Shen, B. Pan, J. Jiao, C. Xia, Kinetic and fluid dynamic modeling, numerical approaches of flowing-gas diode-pumped alkali vapor amplifiers. Opt. Express **23**(15), 19500–19511 (2015)
19. B. Shen, X. Xu, C. Xia, B. Pan, Computation of three-dimensional temperature distribution in diode-pumped alkali vapor amplifiers. Opt. Commun. **368**, 43–48 (2016)
20. B.D. Barmashenko, S. Rosenwaks, K. Waichman, Kinetic and fluid dynamic processes in diode pumped alkali lasers: semi-analytical and 2D and 3D CFD modeling. Proc. SPIE **8962**, 89620C (2014)
21. K. Waichman, B.D. Barmashenko, S. Rosenwaks, Computational fluid dynamics modeling of subsonic flowing-gas diode-pumped alkali lasers: comparison with semi-analytical model calculations and with experimental results. J. Opt. Soc. Am. B **31**(11), 2628–2637 (2014)
22. J. Han, Y. Wang, H. Cai, G. An, W. Zhang, L. Xue, H. Wang, J. Zhou, Z. Jiang, M. Gao, Algorithm for evaluation of temperature distribution of a vapor cell in a diode-pumped alkali laser system (part II). Opt. Express **23**(7), 9508–9515 (2015)